Macro and micro aspects of the transport of chlorides in cementitious membranes

B. Diaz, Xosé Ramon Novoa, Beatriz Puga, Vincent Vivier

Macro and micro aspects of the transport of chlorides in cementitious membranes

B. Díaz[1], X.R. Nóvoa[1,a], B. Puga[1], V. Vivier[2]

[1]ENCOMAT Group, Universidade de Vigo, EEI, Campus Universitario, 36310 Vigo, Spain

[2]LISE- UPR 15 du CNRS, 4 place Jussieu, 75252 Paris Cedex 05, France

[a] corresponding author. E-mail: rnovoa@uvigo.es, Tf: +34986812213

Abstract

A study of the transport of chlorides through hardened Portland cement paste membranes is reported. The flux of chlorides was induced by migration (AC and DC fields) and diffusion.

Two parallel studies were developed. A macroscopic one where the migration of chlorides was followed by Electrochemical Impedance Spectroscopy (EIS) and a microscopic one in which the natural diffusion was investigated using the scanning electrochemical microscopy (SECM). Both studies have revealed to be complementary. The local investigations performed with the SECM were successfully employed for the interpretation of the EIS data.

The results have shown that the transport of chlorides occurs mainly through pores of sub-micrometre equivalent diameter. The study of the transition time has allowed to conclude that the diffusion coefficient approaches the usual value obtained in bulk solution. The macroscopic study has allowed presenting an explanation for the beneficial effect of the AC current in the transport of chlorides. A possible method for estimating the flux of chlorides from the percolation resistance is also discussed.

1. Introduction

The presence of chlorides at the steel/concrete interface level is the main factor responsible for the corrosion of rebars in concrete. In new structures, the penetration rate of chloride ions through the concrete cover is a key aspect in the service life prediction. In damaged structures, the rate of chloride transport is also of major importance for the application of chloride extraction techniques. In that context, the forced migration test is employed as an accelerated and useful method to determine the chloride transport coefficients [1] and several standard methods have been established and used [2, 3]. However, significant microstructural changes are caused by the application of electrics fields [4] that, among other already known aspects dealing with surface treatments [5-7], makes those tests controversial.

Investigations based on electrochemical impedance spectroscopy, EIS, [8, 9] have already evidenced the presence of several concurrent ionic-conduction phenomena in cementitious materials, which involve percolating conduction and ionic exchange between the pore's solution and pore's walls. As each phenomenon occurs at a specific frequency, it is possible to tune the frequency of the electrical signal to act on the conduction paths, thus increasing the current efficiency on the ionic transport and diminishing the structural damage [10]. The use of pulsed current has been reported to be beneficial for preserving the integrity of the concrete microstructure [11].

The chloride diffusion coefficients obtained for concrete either through diffusion or migration experiments are always controversial and strongly dependent on the testing conditions and concrete type [12, 13]. However, all procedures have in common that the amount of transported chlorides is referred to the geometrical surface normal to the transport direction. In neither case the pore structure of the material is taken into account although in some studies a "formation factor" was introduced [14, 15].

The present contribution is aimed at rationalising the macroscopic approaches on the transport of chlorides in the light of microstructural information obtained from impedance spectroscopy measurements and scanning electrochemical microscopy, SECM. A new insight in the field is provided, highlighting the need of microstructural information for reliable results.

2. Experimental

Cement paste samples were prepared using Portland cement type CEM I 52.5R according to the composition, specifications and conformity criteria of EN 197-1:2000, with a water to cement ratio of 0.5. The water-cement mix were cast in cylindrical moulds of 9 cm in diameter and 20 cm in height, and cured in 100% RH chamber for 24 hours. Afterwards, the samples were demoulded and maintained in the same chamber for a minimum of 28 days before starting the measurements. The cement paste samples were cut into 2.5 cm thick slices to be used in the permeation experiments. Unless otherwise stated, the samples were pre-conditioned prior testing following a standardized water saturation procedure [3]. It should be mentioned that the probability for large pores to percolate the sample is almost null. Indeed, the thickness of the samples was chosen to cancel the presence of large percolating pores (inherent in small thicknesses) or cracks (formed during cutting and polishing, due to mechanical stress in thin samples). In this way the samples are representative of the real rebar's cover thickness (larger than 2-3 cm), but are thin enough to develop the microscale experiments within a reasonable and reproducible time scale. The samples microstructure was evaluated using mercury intrusion porosimetry (MIP) performed with an Autopore IV 9500 from Micromeritics. The covered pores diameter range is from 18 μm down to 5 nm.

2.1. Setup for macroscopic permeation experiments

The experimental setup for macro-migration experiments consisted of a classical permeation cell with two-solution compartments at both sides of the cementitious sample under test. The upstream (or cathodic) compartment was filled with 1 M sodium chloride solution, containing also sodium hydroxide and potassium hydroxide to $[OH^-]$ = 0.5 M. The downstream (or anodic) compartment was filled with only sodium hydroxide and potassium hydroxide solutions to $[OH^-]$ = 0.5 M. The concentrations for NaOH and KOH were chosen to be similar to the pH of the pore solutions of the cement. Each electrolyte compartment was 200 cm^3 in volume. A schematic view of the experimental cell is given in Fig. 1.

Figure 1

As depicted in Fig. 1, the AC or DC electric fields were applied to the cementitious membrane using two graphite sheets located at both ends of the cell. The specimens were subjected to two regimes, direct current and pulsed current. In both regimes the nominal current density applied was 0.3 $mA \cdot cm^{-2}$. As the pulsed current was applied as a square wave of 50% duty cycle, the imposed current during the "on" time was 0.60 $mA \cdot cm^{-2}$ to reach the average effective value of 0.3 $mA.cm^{-2}$. The investigated frequency was 1 kHz. In all cases the potential drop across the cell was about 12 V.

The impedance of the cell was measured periodically between 40 MHz and 10 Hz to assess the evolution of the resistivity of the membrane, through which the diffusion coefficient can be derived [8]. The impedance measurements were performed using an Agilent 4294A impedance/gain-phase analyser, which allows impedance frequency range investigation from 100 MHz down to 10 Hz in pure AC mode. This instrument allows capacitance measurements down to 10^{-14} F with a maximum resolution of 10^{-16} F.

The cross-section of the sample in contact with the electrolyte was 20 cm^2 and the measurements were corrected for the ratio sample's geometrical cross section to cross section in contact with the electrolyte as described in [16].

2.2. Setup for microscopic permeation experiments

For micro-diffusion experiments, a specific experimental setup was designed (Fig. 2) in which a 2.5 mm thick cement paste slice acts as membrane between a concentred (0.5 M) KCl solution (upstream compartment) and a diluted (0.01M) KCl solution (downstream compartment). Small amounts (5 mM and 50 mM) of $K_3Fe(CN)_6$ and $K_4Fe(CN)_6$ salts were added to the chlorinated solutions when a redox mediator was required for surface imaging purposes.

Figure 2

The downstream compartment allows the scanning electrochemical microscopy (SECM) experiments to be performed and contains the tip, the counter electrode (a Pt mesh), and the reference electrode (a saturated calomel - SCE).

The flux of chlorides through the cement paste membrane stream compartments was detected using the SECM tip polarised at the appropriate potential. The whole SECM setup used in this work has already been described elsewhere [17, 18].

3. Results

Microstructural characterisations of the samples were performed by mercury intrusion porosimetry. The results depicted in Fig. 3 are in good agreement with those reported for a similar system [19], with two main pore families centred at about 20 and 90 nm in diameter, the overall porosity being about 14%.

Figure 3

3.1. Macroscopic experiments

The flux of chlorides through cementitious membranes is usually split in two regimes: the steady state and the non-steady state regimes [20]. The latter corresponds to the time required for chlorides to reach the downstream compartment, while the former corresponds to the period starting at the end of the non-steady state. Those two periods are clearly identified in Fig. 4 where differential behaviour is observed for the DC and AC regimes. At steady state, the larger slope of the 1 kHz curve indicates that the transport of chlorides is more efficient under AC regime. The fluxes of chlorides obtained directly from the both slopes are 15 µmol.h^{-1} and 6 µmol.h^{-1}, for the AC regime and DC regime, respectively.

Figure 4

During the migration experiments periodic impedance measurements were performed on the cells, after being disconnected from the corresponding power sources and a 15 minute waiting-time as a relaxation period, *i.e.,* the average the time necessary for stabilisation of the potential difference across the samples. A typical impedance diagram is presented in Fig. 5. It was obtained after 30 days under AC regime at 1 kHz. The impedance data were modelled using the equivalent circuit depicted in the inset of Fig. 5. The equivalent impedance is given by Equation 1.

$$Z(\omega) = R_e + \frac{Z_1 \cdot Z_2}{Z_1 + Z_2} \quad (1)$$

where $Z_1 = \frac{R_1}{1 + (j\omega R_1 C_1)^{\alpha_1}}$ (2)

and $Z_2 = R_2 \cdot \left(1 + (j\omega R_2 C_2)^{-\alpha_2}\right)$. (3)

Figure 5

The physical meaning of the parameters in Equation 1 has been reported in Refs [8, 9]. R_e accounts for the electrolyte resistance at both sides of the membrane, R_1 is the resistance associated to the percolating porosity, and C_1 is the geometric capacitance of the sample, corresponding to the solid phase. The time constant R_2C_2 is associated to the ionic exchange between the liquid phase and the pore walls, C_2 being the corresponding double layer capacitance [9, 19]. The dispersion parameters α_1 and α_2 are introduced to account for the Cole-Cole dispersion of the RC time constants. The high dispersion obtained for the R_1C_1 time constant can be attributed to the heterogeneous distribution of the current in the cement paste membrane [16].

The data presented in Fig. 5 show that the electrical model reproduces well the experimental data. The relative error between the experimental impedance data and the fitted values remains below 0.2% in the whole frequency range investigated.. Above 10 MHz the measured impedance is dominated by the series inductance introduced by the graphite electrodes and wires, about 0.4 μH (data not shown). Below 10 kHz, the main contribution to the impedance comes from the interfacial processes at the electrodes. Thus, about three frequency decades are available to study the transport through the cement paste membrane.

Figure 6

The parameter of interest here is R_1, associated to the percolating porosity [8]. The results obtained from the fitting of the impedance spectra with time as parameter are reported in Fig. 6. A continuous increase of the resistance is observed for both regimes from the beginning of the measurement. However, after about 15 days, an inflexion point can be observed on the curve for the DC regime that corresponds to a higher slope and a higher resistance values.

The evolution of the R_1 values in Fig. 6 seems contradictory with a process corresponding to chloride incorporation into the cement because a higher ionic concentration should be associated with a lower resistance, *i.e.* a negative slope as a function of time should have been expected. This apparent contradiction will be discussed later in the section 4.

3.2. Microscopic experiments

The CV curve at 100 mVs^{-1} of the solution with a Pt microelectrode is presented in Fig. 7A, which shows that chloride ions are oxidised at about 1.25 V/SCE. Thus, this potential can be used for the detection of the chlorides arriving from the upstream compartment of the cell. Moreover, at about 0.3V/SCE the reversible response of the ferri/ferrocyanide is evidenced (inset in Fig. 7A). Thus biasing the SECM tip at -0.3 V/SCE (i.e. on the diffusion limited regime for the reduction reaction) allows approach curves (Fig. 7B) and topographic profiles of the cement paste membrane to be performed [21].

Figure 7

3.2.1. Diffusion of chlorides

Starting form a high concentration (0.5M KCl) in the upstream compartment, chlorides could diffuse towards the downstream compartment in which a diluted solution (0.01M KCl) was used. The detection of chlorides flux was performed by cyclic voltammetry between 0.5 and 1.55 V/SCE on the SECM tip as a function of time as shown in Fig. 8A. A continuous increase of the peak current at 1.3V/SCE after 30 minutes was observed, which corresponds to the arrival of chlorides from the upstream compartment.

After verification of the reproducibility of the measurement using different experimental conditions, including using distilled water in the downstream compartment or unsaturated cement paste samples, it was decided to investigate the transport process by performing additional potentiostatic experiments.

Figure 8

Fig. 8B corresponds to an example of the potentiostatic approach. After a fast line scan to locate a pore domain the tip is located in that position and polarised at 1.3V, recording the current as a function of time. The current rise starting at 38 minutes can be associated to the arrival of chlorides which increases the local concentration till about 60 minutes when the diffusion of species into the bulk solution makes the current decrease.

3.2.2. Topography examinations

Topographic profiles of the cement paste surface have been obtained by two different methods: the high frequency conductivity measurement, which is obtained from the electrolyte resistance measurement of the probe and for which no redox mediator is required [22], and the classical negative feedback mode using a mediator (*e.g.* the ferro/ferricyanide redox couple). Both methods provided similar results and only the last one is presented here.

A typical topographic map of the cement paste surface is presented in Fig. 9. The main feature to highlight here is its dynamic nature that can be better noticed through the iso-current surfaces plotted in the X-Y plane. The main pores present have been labelled A to D so that it is possible to qualitatively follow at a glance their evolution with as a function of time from Fig. 9-I to Fig. 9-III.

Figure 9

A quantitative approach to the dynamic behaviour of the interface can be obtained by the integration of the "active surface" at each time on the basis of the identified pores. This integration was performed in Fig. 9 and Fig. 10 using the current contour plots of the XY plane. The results, in percentage of active surface, %S, are 2.6, 5.6 and 2.9, for the initial condition, at 80 minutes and at 410 minutes, respectively. Obviously, these values are only apparent because they depend on the minimum area that can be sense by the SECM tip (lateral resolution), which in turn depends on the tip radius and the tip-to-substrate distance.

The dynamic behaviour of the interface can be understood in terms of dissolution/precipitation processes occurring at the ionic channels. Possible processes are portlandite lixiviation, and precipitation of chloride-containing compounds as Friedel's salt.

Figure 10

Some experiments have been performed using a smaller diameter tip (ϕ = 1 μm) to improve the lateral resolution of the mapping. The results are presented in Fig. 10. Besides the dynamic feature evident when Figs 10I and 10II are compared, more interesting is the percentage of active surface, which is decreased of about one order of magnitude with respect to the values shown in Fig. 9. Such a decrease corresponds to the ratio of the two microelectrodes used for performing experiments presented in Figs. 9 and 10.

This result represents, to our knowledge, the first evidence that the ionic flux through cementitious membranes occurs through pores equal or smaller than 1 μm, which approaches the pore family at 100 nm present in Fig. 3. Several attempts were performed to improve the lateral resolution; however, due to the roughness of the interface, these attempts to use smaller probes failed.

4. Discussion

This last finding allows us to give a reasonable interpretation to the results presented in Fig. 8, and advance an image of the actual meaning of the diffusion coefficient concept in cementitious materials, beyond the "forming factor" usually used in the literature [23,15].

From Fig. 8 data, the transition time, τ, for chlorides through the 2.5 mm thick membrane, d_m, in Equation 4, lies between 30 and 40 minutes which, for linear diffusion, gives a diffusion coefficient, *D*, in the range 6.6 - 8.7x10^{-6} $cm^2.s^{-1}$. Those values are larger than those found for chalk rock using a radiometric method (0.52-3.23 × 10^{-6} cm^2 s^{-1}) [24] and smaller than those for chloride ions in diluted solution (2x10^{-5} $cm^2.s^{-1}$). The difference with diluted solution, a factor 2.3 to 3, can be ascribed to pore tortuosity.

$$D = \frac{d_m^2}{4\tau} \tag{4}$$

For the macroscopic case, the slopes of the curves shown in Fig. 4 at the steady state period correspond to fluxes, *J*, of 2.1x10^{-10} $mol.s^{-1}.cm^{-2}$ and 8.2x10^{-10} $mol.s^{-1}.cm^{-2}$ for the AC and DC regimes, respectively. From these values the corresponding diffusion coefficients, *D*, can be obtained from the Equation 5, and values of 2.2x10^{-8} $cm^2.s^{-1}$ and 0.9x10^{-8} $cm^2.s^{-1}$ are obtained for the AC and DC regimes, respectively. These values lie in the usual experimental range [1], but are three orders of magnitude smaller than those previously discussed for the micro experiments.

$$D = \frac{J}{\frac{zF}{RT} C \frac{\Delta\phi}{\Delta x}} \tag{5}$$

The discrepancy between the micro and macro experiments can however be rationalised if the "active surface" is considered as critical parameter. The active surface, defined as the apparent

cross section of the chloride emitting pores, has been considered to build up Fig. 11. When the pore cross section equals the surface of the macro experiment, both diffusion coefficients are equal. However, when the surface is explored with the tip of ϕ= 10 μm, the active surface represents only 3% of the total surface, as shown in Fig 9. When the surface is explored at higher resolution, with the tip of ϕ= 1 μm, the actual active surface falls to 0.2% (see Fig. 10), which makes the macro-diffusion coefficient values lie in the range of those obtained from the micro experiments. Higher spatial resolution of the SECM tip will be necessary to sense the actual active surface limit, which is as mentioned previously not possible.

Figure 11

The immediate conclusion from these results is that the transport of chlorides through the cement paste membrane involves the porosity below 1 μm pore size, which matches with the pore structure presented in Fig. 3.

In addition, the results presented in Figures 9 and 10 give a clear evidence of the dynamic behaviour of the chloride transport, involving pore blockage, opening and structure changing, as already reported [4, 8]. The dynamic behaviour can be at the origin of the positive slope for the R_1 values in Fig. 6, because the pore blocking can compensate the increase in conductivity due to the ingress of chlorides. More subtle is the difference between AC and DC regimes, also evident in Fig 4.

The dissimilar effect in concrete's microstructure during AC and DC chloride extraction and cathodic protection experiments has already been reported in literature [25, 26]. However, no interpretation to this fact has been given so far. In our opinion, the data reported in the present study allow to advance some causes for the faster ionic transport under AC conditions. As the diffusion coefficient values for ionic motion in the pores approach that of the bulk solution, a characteristic frequency, f_c, for the process of ionic exchange between pore walls and pore solution can be defined by the Equation 6 [27]:

$$f_c = \frac{2D}{\pi\delta^2} \tag{6}$$

where δ represents the pore length along the electric field. As from mercury intrusion porosimetry it is only possible to access the connecting pore necks [28], it is probable that the pore lengths involved in the motion associated to the electric field are higher than the 0.1 μm threshold pore

diameter in Fig. 3. Thus, if D = 10^{-5} $cm^2.s^{-1}$ we get, from Equation 6, a range of f_c between 0.6 kHz and 60 kHz for the limiting lengths ranging from 1 μm and 0.1 μm, respectively.

The application of an AC field, provided it is in the range of f_c, will induce local stirring effects that will make difficult the adsorption process involved in the formation of chloride rich phases (Friedel's salt) [29], hence the local free chloride concentration will be higher and the transport more efficient, which explains the differences observed in Figs. 4 and 6.

Another interesting relationship between the percolation resistance R_1 (Fig. 6) and the flux of chlorides (Fig. 4) under different regimes can be derived from the application of the Nernst-Einstein relation for the ionic transport through membranes [30]. The ionic flux, ϕ, is given by Equation 7, which is independent of the geometry of the membrane :

$$\Phi = \frac{RT}{F^2 R_1} \tag{7}$$

At T= 298 K, and taking R= 8.31 $J \cdot K^{-1}.mol^{-1}$, and F= 96500 $C \cdot mol^{-1}$, Equation 7 gives:

$$\Phi = \frac{958}{R_1(\Omega)} \frac{\mu eq.}{h} \tag{8}$$

Data presented in Fig. 6 have been re-written in terms of flux through Equation 8 and compared with the flux data from chemical analysis (Fig. 4), all in Table 1. The conclusion from these data is that the flux under AC regime is higher than under DC conditions. As at the steady-state period most of the porosity is filled with the electrolyte, the discrepancies between the electrochemical data and the actual flux (the slope obtained analytically) can be viewed as the reaction of chlorides with the pore walls, which is more important for the DC regime. Indeed, after 34 days a good agreement was obtained between the electrochemical and chemical data (40.9 $\mu mol \cdot h^{-1}$ and 39.0 $\mu mol \cdot h^{-1}$, respectively) for the AC regime.

Table 1

The study of R_1 opens the possibility of knowing the flux of chlorides from the environment to the rebar in reinforced concrete structures. This knowledge could be of importance in the definition of the critical chloride concentration for pit initiation. The data available so far, on the basis of chlorides to cement ratio, are highly dispersed [31] without any apparent rationale. Thus, a new

deal could be introduced by combining information on the empty space at the rebar's level and the ionic flux to that space to reach the critical concentration.

5. Conclusions

The SECM technique has been applied for the first time to the study of the transport of chlorides through cementitious membranes. The results presented show that the transport of chlorides occurs mainly through pores of sub-micrometre diameter. The study of the transition time has allowed concluding that the diffusion coefficient approaches the value usually obtained in bulk solution.

Moreover, the SECM study has evidenced the dynamic character of the chloride transport that involves pore blockage and pore opening. This dynamics allowed interpreting the macroscopic results on the variation of the percolation resistance with time. The resistance increases due to blockage of the porosity.

The macroscopic study, mainly based on EIS, has also allowed to present here an interpretation that explains the beneficial effect of the AC current in the transport of chlorides. A possible method for estimating the flux of chlorides was too presented.

Acknowledgement

The Spanish authors would like to thank the Spanish Government for partially funding this work under project #BIA2010-16950. The European Regional Development Fund is also acknowledged for financing the DURATINET project nr. 2008-1/049.

References

[1] K.D. Stanish, R. D. Hooton, M.D.A. Thomas, Testing the chloride penetration resistance of concrete: A literature review, Federal Highway Administration (USA), Publication No. FHWA-RD-00-142 (2000).

[2] AASHTO T 277-07 (2011), Standard Method of Test for Electrical Indication of Concrete's Ability to Resist Chloride Ion Penetration, American Association of State Highway and Transportation

Officials (AASHTO), Standard Specifications for Transportation Materials and Methods of Sampling and Testing, 32nd edition 2012, page T 277-1 volume 2B.

[3] ASTM C1202 (2012), Standard Test Method for Electrical Indication of Concrete's Ability to Resist Chloride Ion Penetration, American Society for Testing and Materials (ASTM) volume 04.02 Concrete and Aggregates, 2012.

[4] I. Sáchez, X. R. Nóvoa, G. de Vera, M. A. Climent, Microstructural modifications in Portland cement concrete due to forced ionic migration tests. Study by impedance spectroscopy. Cem. Conc. Res. 38 (2008) 1015–1025.

[5] C. Andrade, D. Whiting, A comparison of chloride ion diffusion coefficients derived from concentration gradients and non-steady state accelerated ionic migration, Mater. Struct. 29 (1996) 476-484.

[6] C. C. Yang, A comparison of transport properties for concrete using the ponding test and the accelerated chloride migration test, Mater. Struct. 38 (2005) 313-320.

[7] Seyoon Yoon, Sang-gyun Oh, Juyoung Ha, P. M. Monteiro, The effects of surface treatments on rapid chloride permeability tests, Mat. Chem. Phys. 135 (2012) 699–708.

[8] B. Díaz, X.R. Nóvoa, M.C. Pérez, Study of the chloride diffusion in mortar: A new method of determining diffusion coefficients based on impedance measurements, Cem. Conc. Comp. 28 (2006) 237-245.

[9] M. Cabeza, P. Merino, A. Miranda, X.R. Nóvoa, I. Sánchez, Impedance spectroscopy study of hardened portland cement paste, Cem. Conc. Res. 32 (2002) 881–891.

[10] B. Díaz, X.R. Nóvoa, B. Puga, V. Vivier, Chloride transport through cementitious membranes using pulsed current, Cem. Conc. Comp. (submitted)

[11] D.A. Koleva, O. Copuroglu, K. van Breugel, G. Ye, J.H.W. de Wit, Electrical resistivity and microstructural properties of concrete materials in conditions of current flow, Cem. Conc. Comp. 30 (2008) 731–744.

[12] J. Gergely, J. E. Bledsoe, B. Q. Tempest, I. F. Szabo, *Concrete Diffusion Coefficients and Existing Chloride Exposure in North Carolina*. No. FHWA/NC/2006-26. Department of Civil Engineering, University of North Carolina at Charlotte, 2006.

[13] Ha-Won Song, Chang-Hong Lee, Ki Yong Ann, Factors influencing chloride transport in concrete structures exposed to marine environments, Cem. Conc. Comp. 30 (2008) 113–121.

[14] K.A. Snyder, The relationship between the formation factor and the diffusion coefficient of porous materials saturated with concentrated electrolytes: theoretical and experimental considerations, Concr. Sci. Eng. 3 (2001) 216–224.

[15] H. Mercado, S. Lorente, X. Bourbon, Chloride diffusion coefficient: A comparison between impedance spectroscopy and electrokinetic tests, Cem. Conc. Comp. 34 (2012) 68–75.

[16] B. Díaz, L. Freire, X. R. Nóvoa, B. Puga, V. Vivier, Resistivity of cementitious materials measured in diaphragm migration cells: the effect of the experimental set-up, Cem. Conc. Res. 40 (2010) 1465–1470.

[17] C. Gabrielli, F. Huet, M. Keddam, P. Rousseau, V. Vivier, Scanning electrochemical microscopy for investigating gas bubble/liquid interfaces, Electrochem. and solid-state letters 6 (2003) E23-E26.

[18] C. Gabrielli, S. Joiret, M. Keddam, H. Perrot, N. Portail, P. Rousseau, V. Vivier, Development of a coupled SECM-EQCM technique for the study of pitting corrosion on iron, J. Electrochem. Soc. 153 (2006) B68-B74.

[19] M. Cabeza, P. Merino, X.R. Nóvoa, I. Sánchez, Electrical effects generated by mechanical loading of hardened Portland cement paste, Cem. Conc. Comp. 25 (2003) 351–356.

[20] X. Shi, N. Xie, K. Fortune, J. Gong, Durability of steel reinforced concrete in chloride environments: An overview, Const. Build. Mater. 30 (2012) 125–138.

[21] A. J. Bard, M. V. Mirkin, Scanning Electrochemical Microscopy, CRC Press, 2001, pp. 111-124.

[22] C. Gabrielli, F. Huet, M. Keddam, P. Rousseau, V. Vivier, Scanning Electrochemical Microscopy Imaging by Means of High-Frequency Impedance. Measurements in Feedback Mode, J. Phys. Chem. B, 108 (2004) 11620-11626

[23] K. A. Snyder, The relationship between the formation factor and the diffusion coefficient of porous materials saturated with concentrated electrolytes: theoretical and experimental considerations. Concr. Sci. Eng. 3 (2001) 216-224.

[24] D. Hill, Diffusion coefficients of nitrate, chloride, sulphate and water in cracked and uncracked Chalk, J. Soil Sci., 35 (1984) 27-33.

[25] D. A. Koleva, J. Hu, K. van Breugel, N. Boshkov, H. de Wit, Conventional and Pulse Cathodic Protection of Reinforced Concrete: Electrochemical Approach and Microstructural Investigations. ECS Transactions, 1 (2006) 287-298.

[26] D. A. Koleva, J. H. W. De Wit, K. Van Breugel, Z. F. Lodhi, G. Ye, Investigation of Corrosion and Cathodic Protection in Reinforced Concrete II. Properties of Steel Surface Layers, J. Electrochem. Soc. 154 (2007) C261-C271.

[27] C. Alonso, C. Andrade, M. Keddam, X. R. Nóvoa, H. Takenouti, Study of the dielectric characteristics of cement paste, Mater. Sci. Forum, 289-292 (1998) 15-28.

[28] R. A. Cook, K. C. Hover, Mercury porosimetry of hardened cement pastes, Cem. Conc. Res. 29 (1999) 933-943.

[29] A. K. Suryavanshi, J. D. Scantlebury, S. B. Lyon, Mechanism of Friedel's salt formation in cements rich in tri-calcium aluminate, Cem. Conc. Res. 26 (1996) 717-727.

[30] M. H. Gottlieb, K. Sollner, Failure of the Nernst-Einstein equation to correlate electrical resistances and rates of ionic self-exchange across certain fixed charge membranes, Biophys. J. 8 (1968) 515-535.

[31] U. Angst, B. Elsener, C. K. Larsen, Ø. Vennesland, Critical chloride content in reinforced concrete - a review, Cem. Conc. Res. 39 (2009) 1122-1138.

Data from R_1 (Fig. 6)				Data from the slopes (Fig. 4)
	At 22 days	At 24 days	At 34 days	Slope conc./time
AC (1kHz) mode	68.7	66.1	40.9	39.0
DC mode	48.9	47.0	21.6	15.6

Table 1. Flux of chlorides, in $\mu mol.h^{-1}$, through the cement paste membrane obtained from R_1 data (Fig. 6) using equation 8, and from the slopes in Fig 4.

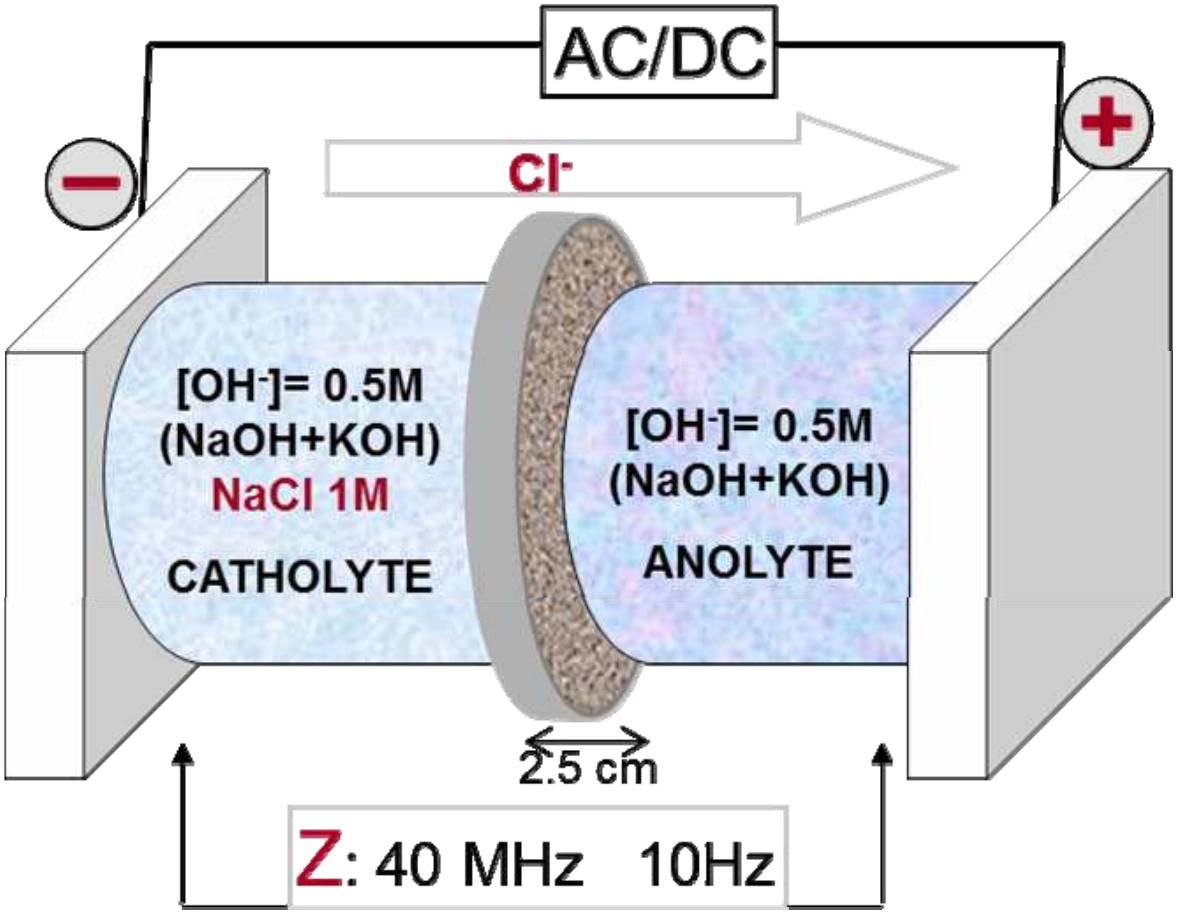

Figure 1. Schematic view of the experimental permeation cell employed for the macroscopic experiments. Each compartment is 10 cm in length and 5 cm in diameter, thus containing 200 cm^3 solution in each compartment with a cross section area of 20 cm^2.

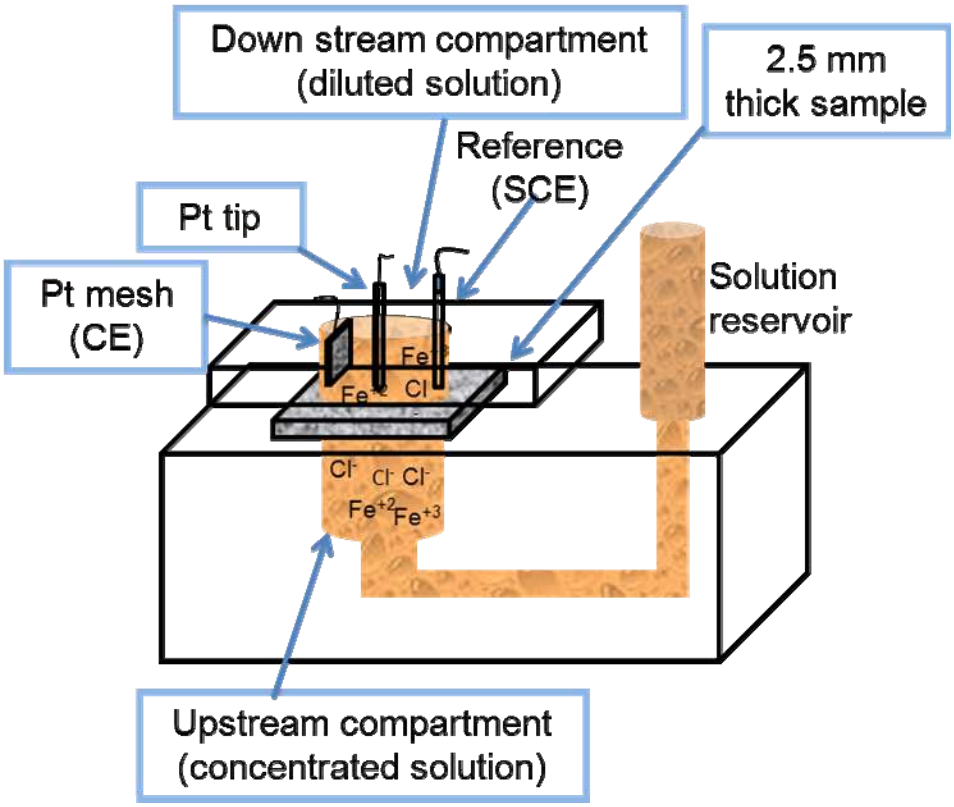

Figure 2. Schematic view of the experimental permeation cell employed for the microscopic experiments of natural diffusion.

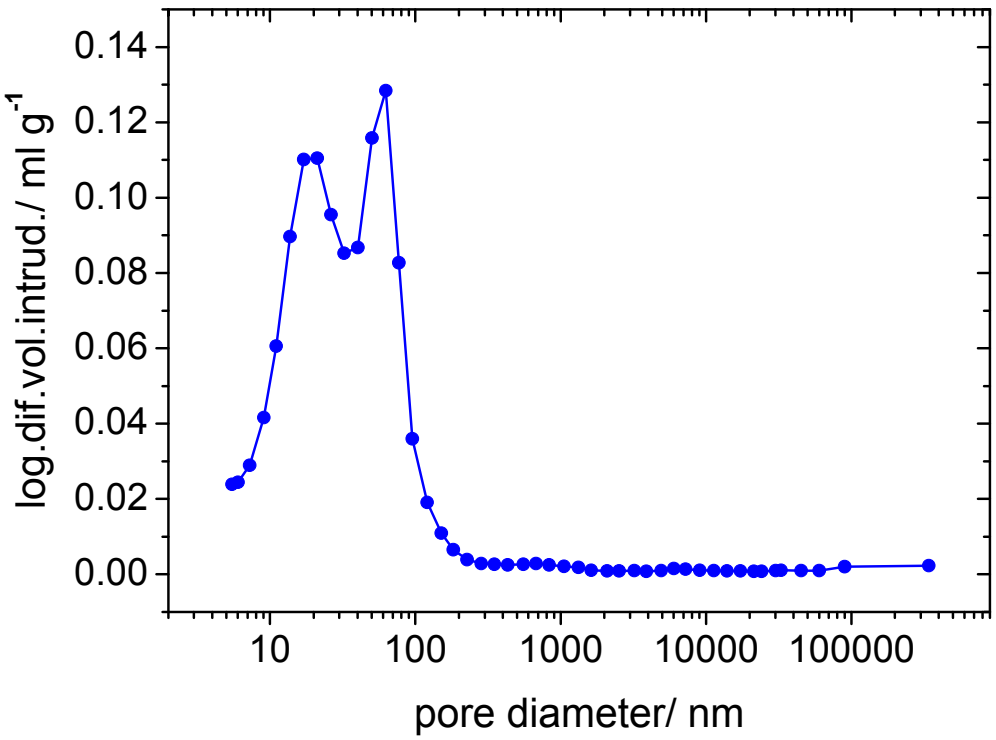

Figure 3. Example of the pore size distribution obtained by mercury intrusion porosimetry, i.e. logarithm of the differential intruded volume ($ml.g^{-1}$) vs. pore diameter (nm), for a hardened cement paste with 0.5 water to cement ratio, after 30 days of curing time.

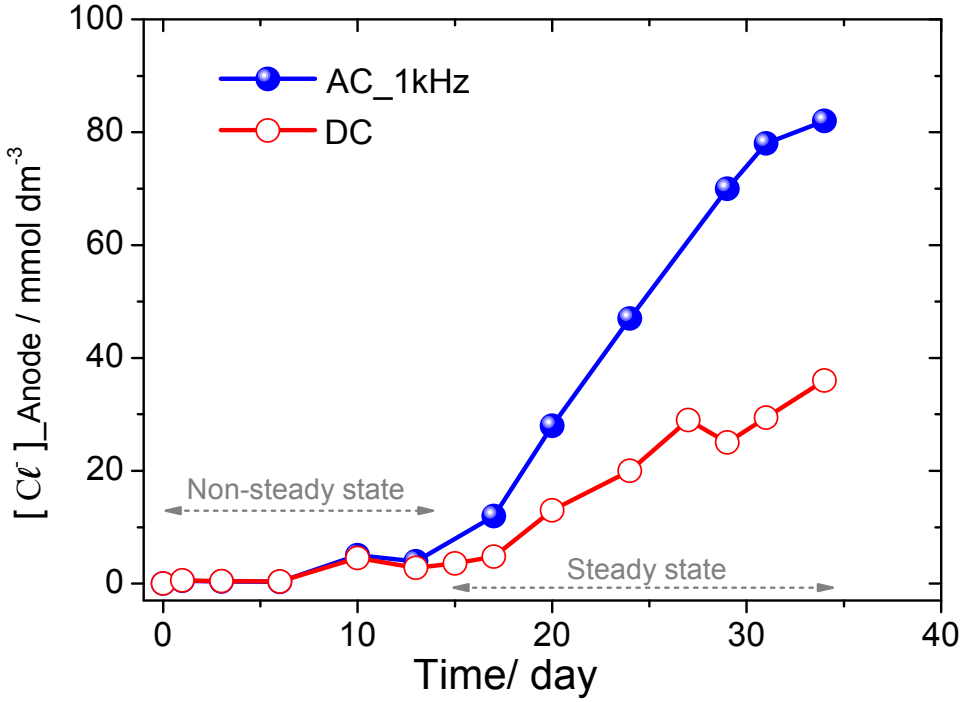

Figure 4. Concentration of chlorides in the anode side (200 cm^3 downstream compartment) as a function of the treatment time under DC and AC (1 kHz) regimes.

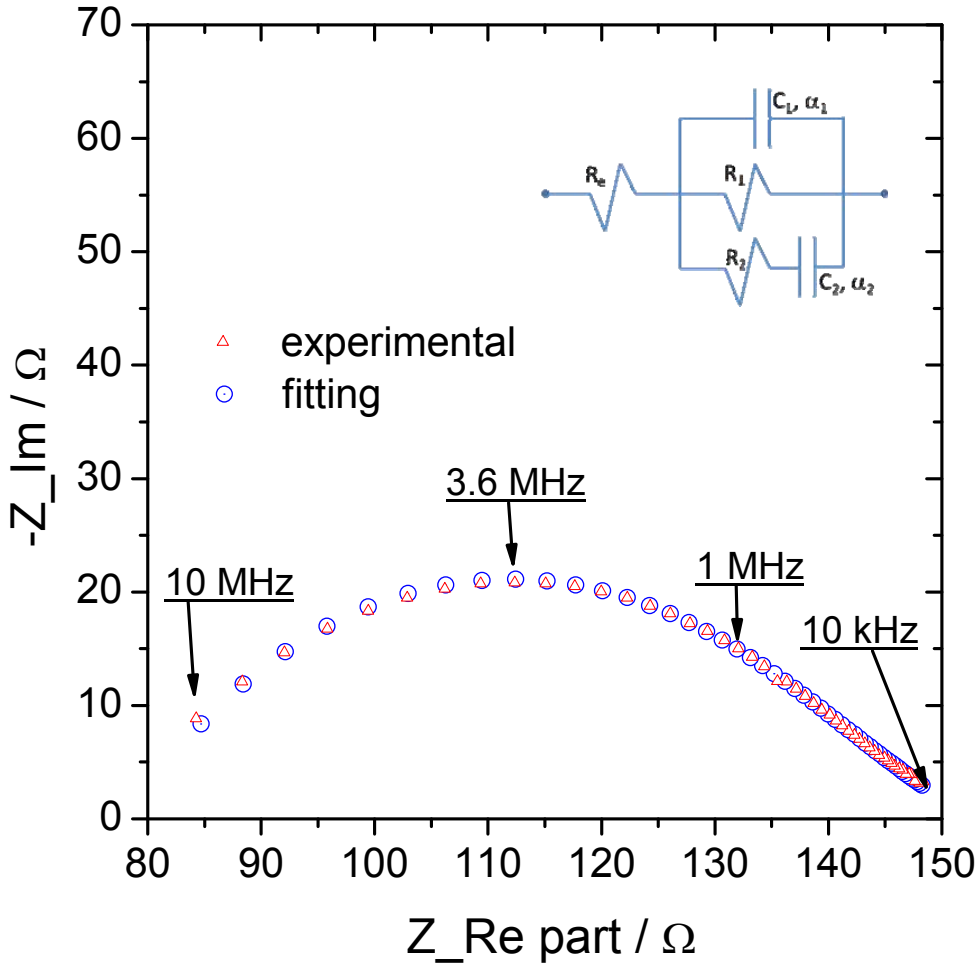

Figure 5. Nyquist impedance spectrum obtained for a sample treated at 1 kHz for 30 days. The corresponding best fitting results (open circles) to equation 1 are also given. The best fitting parameters are: R_e= 44 Ω, R_1= 108.5 Ω, C_1 = 24.8 pF, α_1= 0.38, R_2= 10.4 Ω, C_2 = 140.3 pF, α_2= 0.96. An uncompensated series inductance of 0.4 µH corresponding to the wiring arrangement (mainly the electrode graphite sheets) has been considered in the fitting.

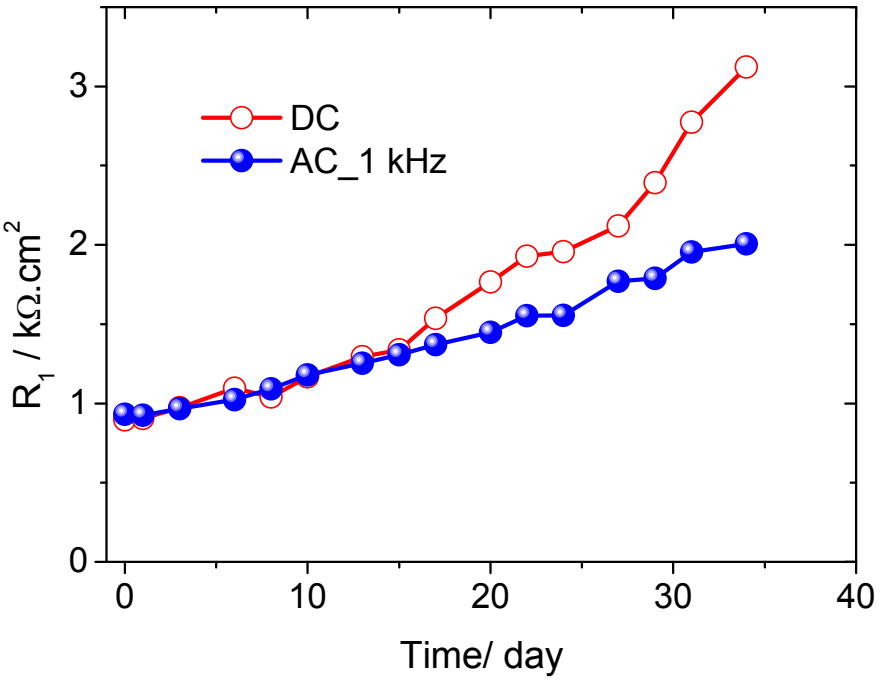

Figure 6. Evolution of the percolation resistance R_1 as a function of time for a DC and AC (1 kHz) regimes.

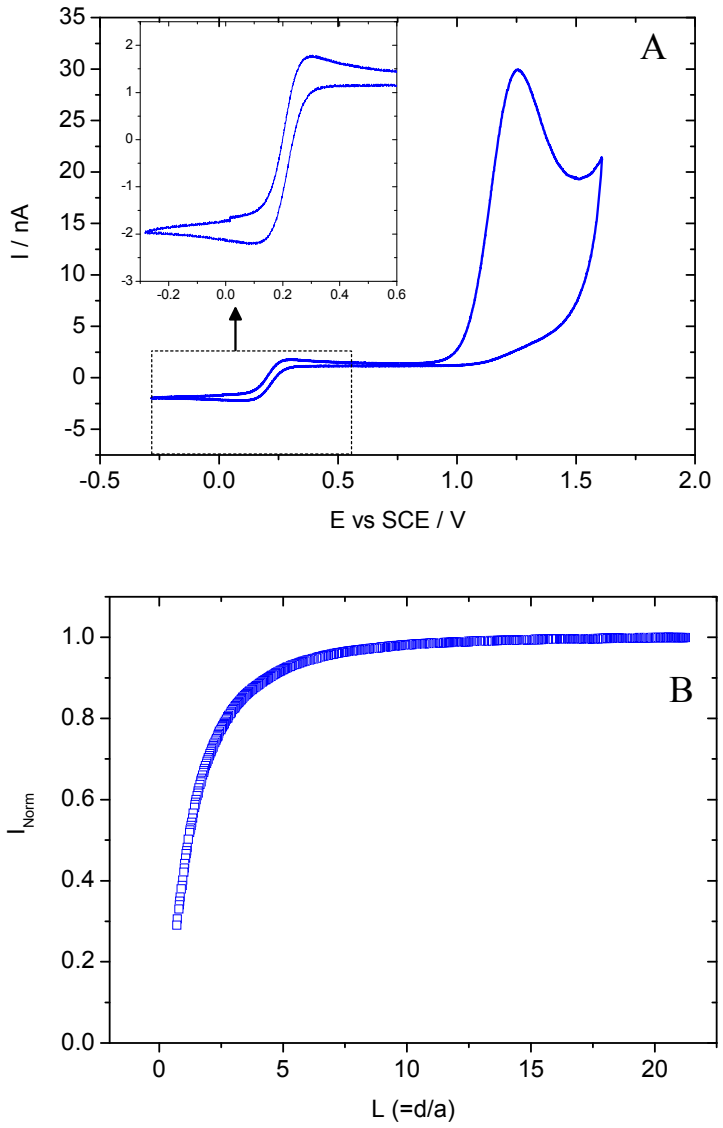

Figure 7. Electrochemistry on a 10 µm diameter SECM tip immersed in the downstream compartment solution containing 10 mM $K_3Fe(CN)_6$ and 0.5 M KCl.

A) Cyclic voltammetry performed at 100 $mV.s^{-1}$.

B) Approach curve performed on negative feedback mode (tip polarised at -0.3V/SCE). The tip-sample distance, d, corresponds to the normalised distance, L, times de radius of the tip, a.

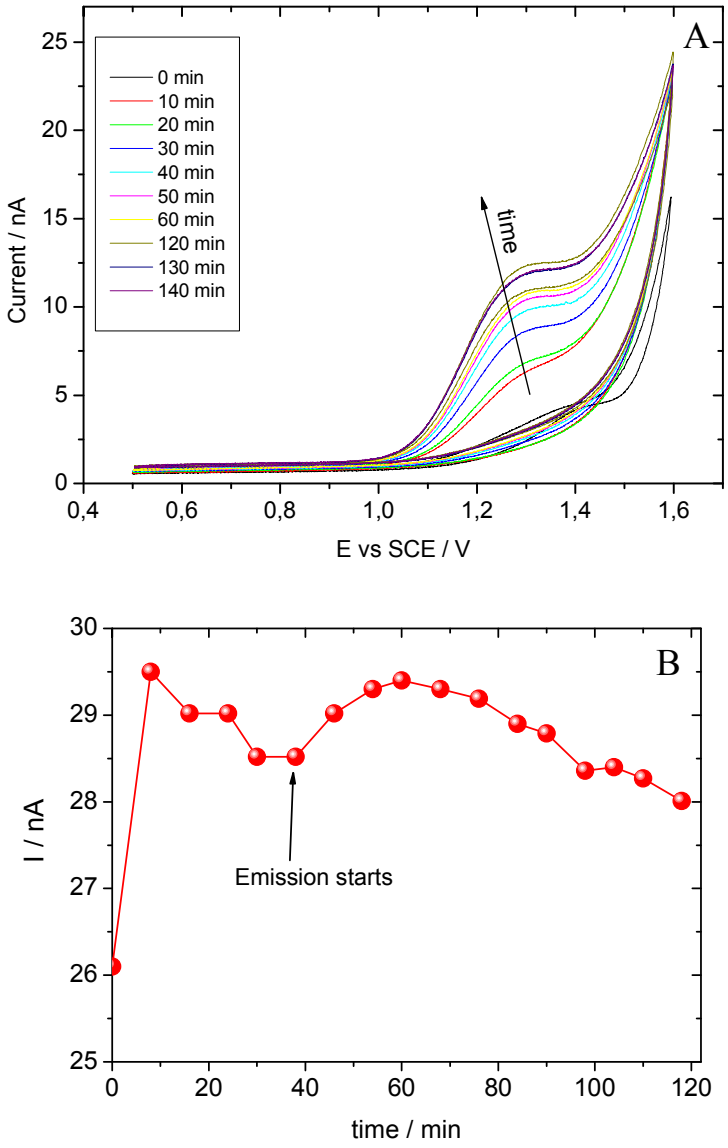

Figure 8. Electrochemistry on a 10 µm diameter SECM tip placed close to the cement paste sample. The upstream compartment solution containing 10 mM $K_3Fe(CN)_6$ and 0.5 M KCl. The downstream solution (compartment of the SECM tip) was 5 mM $K_3Fe(CN)_6$ and 0.01 M KCl.

A) Temporal series of cyclic voltammetries performed at 50 $mV.s^{-1}$.

B) Evolution of the tip current with immersion time. Tip polarised at +1.3V vs. SCE and positioned on a pore, as determined by previous fast line-scan topography, L= 1.14.

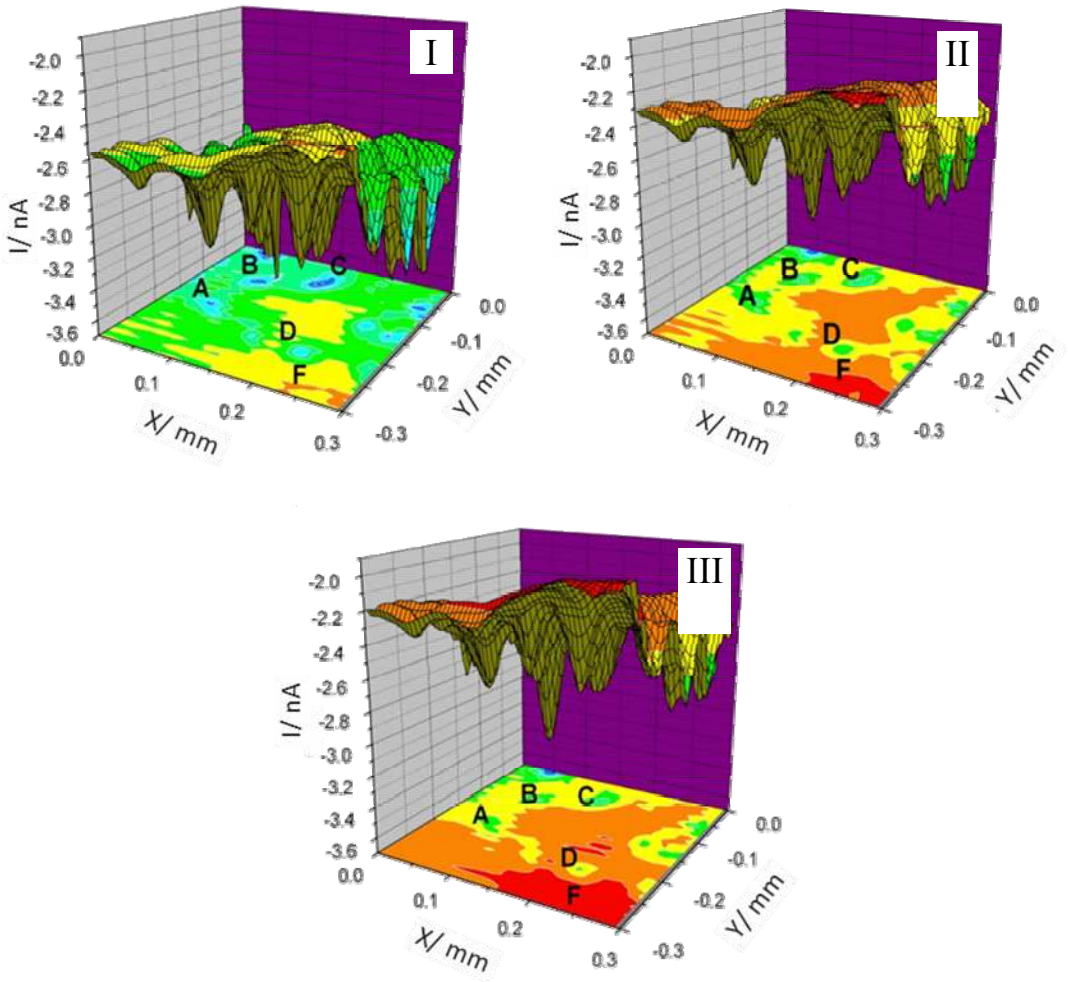

Figure 9. Topographic maps of the cement paste membrane obtained as a function of time. The downstream compartment solution containing 5 mM $K_3Fe(CN)_6$ + 0.01 M KCl. The downstream compartment solution containing 10 mM $K_3Fe(CN)_6$ + 0.5 M KCl. The diameter of the tip was Ø= 10 µm, the sweep rate υ=10 µm.s^{-1}, L=0.8, and E_{tip}=-0.3V vs.SCE.

I) Initial condition. $\%S_{active}$ = 2.6 (see text).

II) At 80 minutes. $\%S_{active}$ = 5.6 (see text).

III) At 410 minutes. $\%S_{active}$ = 2.9 (see text).

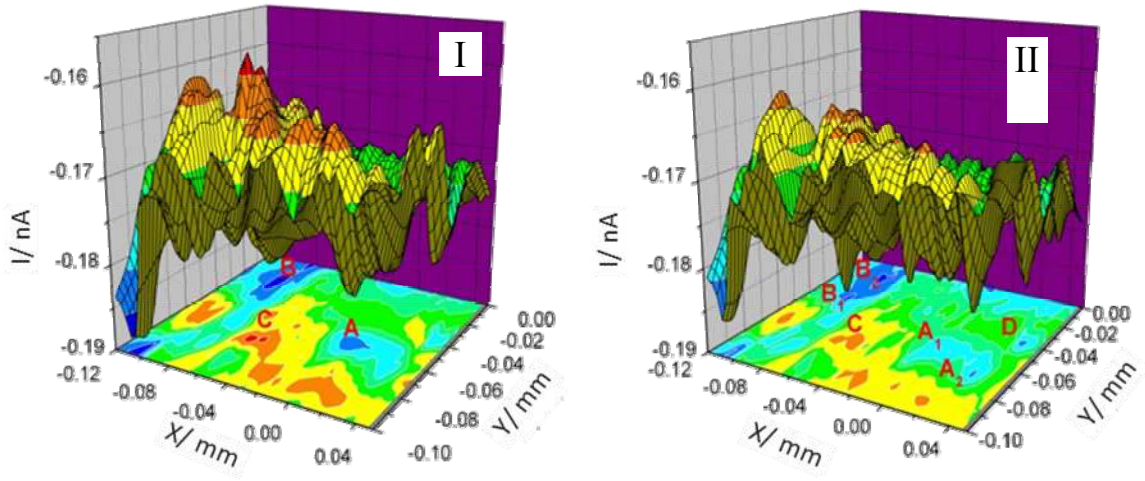

Figure 10. Topographic maps of the cement paste membrane obtained as a function of time. The downstream compartment solution containing 5 mM $K_3Fe(CN)_6$ + 0.01 M KCl. The downstream compartment solution containing 10 mM $K_3Fe(CN)_6$ + 0.5 M KCl. The diemeter of the tip was Ø= 1 µm, the sweep rate υ=5 µm.s^{-1}, L=1.9, and E_{tip}=-0.3V vs.SCE.

I) At 360 minutes. $\%S_{active}$ = 0.3 (see text).

II) At 480 minutes. $\%S_{active}$ = 0.1 (see text).

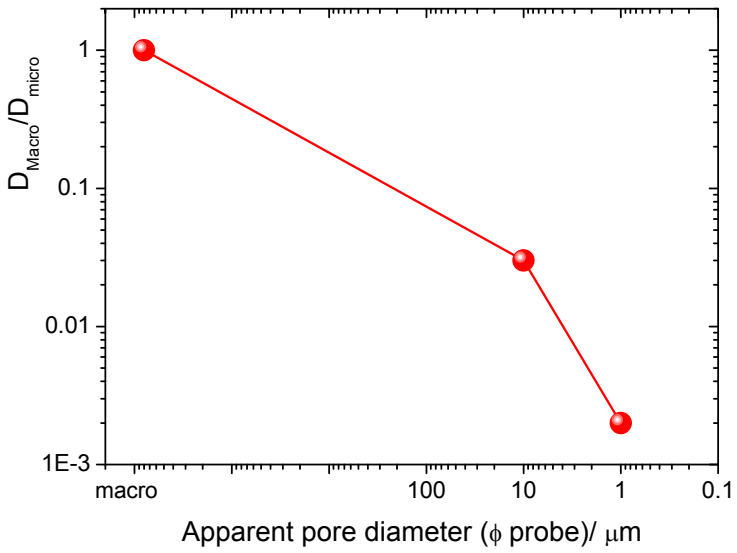

Figure 11. Dependence of the measured diffusion coefficient on the apparent size of the emitting pores.